Original Article

Bioinformatics analysis based on ferroptosis-related lncRNAs: construction of a clinical prognostic model for nasopharyngeal carcinoma and correlation analysis

Zuwen Dai, Yi Zhong

Department of Otolaryngology, Zhejiang Quhua Hospital, Quzhou, China

Contributions: (I) Conception and design: Z Dai; (II) Administrative support: Z Dai; (III) Provision of study materials or patients: Z Dai; (IV) Collection and assembly of data: Y Zhong; (V) Data analysis and interpretation: Y Zhong; (VI) Manuscript writing: Both authors; (VII) Final approval of manuscript: Both authors.

Correspondence to: Zuwen Dai. Department of Otolaryngology, Zhejiang Quhua Hospital, Quzhou, China. Email: daizuwen136@163.com.

Background: A prognostic model of ferroptosis associated with long non-coding RNAs (lncRNAs) in nasopharyngeal carcinoma was established by using The Cancer Genome Atlas (TCGA) database, and immune correlation analysis was conducted for patients classified into high- and low-risk groups by the model. Nasopharyngeal carcinoma is associated with many lncRNA gene mutations, and tumors are often closely related to metabolism, accompanied by obvious characteristics of immune infiltration.

Methods: Gene expression data and clinical data of nasopharyngeal carcinoma tissues and normal tissues were obtained from TCGA database, and differential lncRNAs related to ferroptosis were screened out. Univariate and multivariate Cox risk regression models were used to screen and establish the lncRNA prognostic risk prediction model. Patients were scored according to the model. The immune-related functions of the high-risk and low-risk groups were compared to obtain immune-related differences between the groups. In this study, the prognostic model was constructed by the intersection of genes related to nasopharyngeal cancer prognosis and genes related to iron death metabolism through Cox regression analysis and R-packet screening, and the area under curve (AUC) was further used to predict and verify the model.

Results: In this study, a total of 14 differential lncRNAs related to the prognosis of ferroptosis were obtained. Immune correlation analysis showed that the high- and low-risk groups had significant differences in the following factors: dendritic cells, B cells, mast cells, and other immune cells (P=0.0001); anaphase-promoting complex (APC) co-inhibition, chemotactic factor receptor, immune checkpoint, and other immune functions (P=0.002); glutamate cysteine ligase catalytic (GCLC), human endogenous retrovirus-H long terminal repeat-associating protein 2 (HHLA2), cluster of differentiation (CD276), B and T-lymphocyte attenuator (BTLA), and other immune checkpoint related genes (P<0.001). GCLC was highly expressed in NP69/DDP cells (P=0.04). DDP can activate ferroptosis in NP69/DDP cells can inhibit GCLC expression, and the AUC curve (AUC =0.899) indicates that the model has good prediction and accuracy.

Conclusions: The prognostic model based on 16 ferroptosis-related lncRNAs can predict the prognosis of nasopharyngeal carcinoma patients, and the ferroptosis-related lncRNAs involved in the construction of the model obtained in this study may be related to the level of immune infiltration, and may even become new targets for immune checkpoint inhibitor therapy.

Keywords: Nasopharyngeal carcinoma; ferroptosis; long non-coding RNA (lncRNA); prognosis of survival; immunotherapy

Submitted Mar 30, 2022. Accepted for publication Jun 14, 2022.
doi: 10.21037/tcr-22-1196
View this article at: https://dx.doi.org/10.21037/tcr-22-1196

Introduction

Nasopharyngeal carcinoma is a common malignant tumor with one of the highest morbidity and mortality rates worldwide (1). The mechanism of the occurrence and development of nasopharyngeal carcinoma is still not completely clear, and the treatment of nasopharyngeal carcinoma is still a major problem to be solved (2). Iron is one of the essential trace elements in the human body (3). It is involved in various biological processes (BPs), including hemoglobin synthesis, oxygen transport, DNA synthesis, and oxidation emergency response, among others. Ferroptosis is also an important BP related to cell death (4). In the past, there were 3 known main processes of cell death, namely necrosis, autophagy, and apoptosis. In recent years, with continuous in-depth research, new pathways and processes of cell death have been discovered, such as cell pyroptosis and ferroptosis. Ferroptosis is a kind of programmed cell death dependent on iron ions, which is different from other forms of cell death such as apoptosis (5). Its mechanism is that overloaded iron divalent ions in the cell make the cell produce a large number of lipid reactive oxygen species (ROS), which leads to the accumulation of lipid peroxides and induces ferroptosis. Studies have found that ferroptosis is generally inhibited in lung cancer cells, and the molecular mechanisms involved are not fully understood (6-8). Inducing cell death is considered a viable cancer treatment, and ferroptosis is also considered a potential therapeutic strategy to trigger cancer cell death, especially for malignancies that are resistant to conventional therapies (9).

Long non-coding RNAs (lncRNAs) are long non-protein coding RNAs with a nucleotide length >200. LncRNAs are involved in many BPs including gene transcription, translation, and regulation and mRNA degradation. LncRNAs play a major regulatory role in many disease processes including cancer (10). LncRNAs are key mediators of ferroptosis and iron metabolism in cancer. They may form a specific regulatory network with mRNAs, miRNAs, and other related molecules and jointly participate in the process of ferroptosis in cancer cells, and also play an important role in the occurrence, development, and prognosis of cancer. Glutamate cysteine ligase catalytic (*GCLC*) gene can promote the proliferation and metastasis of nasopharyngeal carcinoma cells. Inhibition of GCLC expression in nasopharyngeal carcinoma cells can significantly enhance their sensitivity to chemotherapy drugs. These findings suggest that the occurrence of ferroptosis regulated by GCLC may be related to the chemotherapeutic drug resistance of tumor cells. Therefore, this paper takes GCLC-mediated ferroptosis as the entry point to study the role of GCLC-mediated ferroptosis in NP69/DDP resistance, providing a theoretical basis for the clinical treatment of nasopharyngeal carcinoma (11-13). Ferroptosis is an iron-dependent lipid reactive oxygen species, which is different from apoptosis, cell necrosis, pyrosis and autophagy. Regulated cell death (RCD) pathway mediated by L-ROS. The main mechanism is that Fe2+ transfers electrons to oxygen atoms in the cell, which produce ROS, resulting in the peroxidation of phospholipid molecules in the long-chain unsaturated fatty acids on the membrane or organelle membrane, resulting in the formation of lipide peroxide (LPO), and then the thinning and curvature of the biofilm. Causing the cell membrane to rupture and the cell to die. A new type of oxygenated modulator cell death driven by iron dependent lipid peroxidation, distinguished from apoptosis, cell necrosis and autophagy, was named “iron death”. Iron death was defined by three basic markers: (I) oxidation of membrane phospholipids containing polyunsaturated fatty acids; (II) availability of REDOX active iron; (III) loss of repair ability of lipid hydrogen peroxide. Iron death plays an important role in human physiological development, internal microenvironment balance and diseases. In physiological and pathological states, iron death can be caused by various internal and external environmental factors as well as social and psychological factors. Iron death is therefore closely associated with clinical conditions such as cancer, cerebral hemorrhage, and traumatic brain injury.

In this study, a prognostic model of ferroptosis-related lncRNAs in nasopharyngeal carcinoma was constructed by using The Cancer Genome Atlas (TCGA) database, and the correlation between ferroptosis-related lncRNAs and the prognosis of nasopharyngeal carcinoma patients was systematically evaluated (14). In addition, the high-risk and low-risk groups were compared in terms of immune function, and we further explored the related drug tolerance to nasopharyngeal carcinoma immunosuppressant therapy. Our findings provide a new train of thought and theoretical basis for future studies in this field. We present the following article in accordance with the TRIPOD reporting checklist (available at https://tcr.amegroups.com/article/view/10.21037/tcr-22-1196/rc).

Methods

Data source

The gene expression levels and clinical data in this study were obtained from TCGA nasopharyngeal carcinoma dataset. The data of medium gene expression were obtained from 535 tumor samples and 59 normal samples, and the clinical data included the clinical information of 522 patients with nasopharyngeal carcinoma, such as the state of existence, the time of existence, and the tumor stage. Ferroptosis-related genes from the FerrDb (http://www.zhounan.org/ferrdb/) database yielded a total of 257 genes. First, target lncRNAs related to patient prognosis were preliminarily screened by univariate Cox regression analysis (Filter criteria: P<0.05). Lasso regression was performed again to further screen and analyze the data to reduce over-fitting and screen the key lncRNAs associated with iron death. Cross-validation was used to select parameters for Lasso regression, and Lasso regression coefficient spectrum was drawn. Finally, multivariate Cox regression analysis was performed to establish iron death-related lncRNA models with value for disease prognosis. The model formula was used to calculate the risk value of the samples. According to the median value, the samples were divided into two groups with high and low risk for survival difference analysis. Kaplan-Meier curve, risk heat map and risk score are drawn to evaluate the ability of predicting patient survival of the model. Then, independent prognostic analysis was conducted after the combination of Risk score and clinical data to prove whether the model could be used as an independent prognostic factor of patients independent of other clinical traits. Finally, statistical analysis was conducted on clinical data through the Risk score of clinical factors. The study was conducted in accordance with the Declaration of Helsinki (as revised in 2013).

Extraction of ferroptosis-related lncRNAs in nasopharyngeal carcinoma

According to annotated files of the human genome downloaded from Gencode (https://www.gencodegenes.org), mRNAs and lncRNAs were distinguished from RNA-seq data of nasopharyngeal carcinoma patients in TCGA database. A total of 19,604 mRNAs and 14,086 lncRNAs were obtained. The expression matrix of 245 ferroptosis-related genes in nasopharyngeal carcinoma was obtained by the intersection of 257 ferroptosis-related genes with the RNA-seq data of nasopharyngeal carcinoma patients in TCGA database using the limma package in R language. P<0.001 for filtering were used to determine the significant ferroptosis-related lncRNAs.

Differential expression analysis

Using the limma package in R language, the lncRNAs significantly associated with ferroptosis were tested by the Wilcoxon test, and set the filter conditions to |logFC| >1, q<0.05. Differentially expressed ferroptosis-related lncRNAs in tumor and normal samples were obtained. Combined with TCGA clinical data, univariate Cox regression analysis was performed on the differentially expressed lncRNAs. P<0.05 was considered to be statistically significant, and the difference in prognosis of ferroptosis was obtained.

Construction of the prognostic risk prediction model

The lncRNAs showing a significant difference in the prognosis of ferroptosis obtained by univariate Cox regression analysis were incorporated into the multivariate Cox regression analysis to construct a multivariate prognostic risk prediction model. The risk score of each patient was calculated according to the model, and the patients were divided into high- and low-risk groups based on the median of the risk score. Then, the survival package and time ROC package of R language were used to verify and evaluate the prognostic risk prediction model.

Enrichment analysis

The "ClusterProfiler" and "org.hs.eg.db" packages in R language were used to perform Gene Ontology (GO) and Kyoto Encyclopedia of Genes and Genomes (KEGG) analyses, respectively, and GO enrichment analysis was used to analyze the main functions of the mRNAs with differential expression. GO enrichment analysis included cellular component (CC) and molecular function (MF), etc. KEGG enrichment analysis was used to analyze the main enrichment pathways of differentially expressed mRNAs.

Analysis of immune function status

TCGA nasopharyngeal carcinoma infiltration results were downloaded from the Timer 2.0 database (http://timer.comp-genomics.org/). The "ssGSEA" package in R language was used to quantitatively calculate the immune cell infiltration fraction and activity of immune-related

functions in the high- and low-risk groups based on the lncRNA prognostic risk prediction model, and analyze their immune function status.

Cells and reagents

The human nasopharyngeal carcinoma cell line (NP69) and human nasopharyngeal carcinoma DDP drug-resistant strain (NP69/DDP) were purchased from Shanghai Cell Bank, Chinese Academy of Sciences. RPMI-1640 medium, streptomycin, penicillin, and 0.25% trypsin were purchased (Hyclone Company, USA). The ROS detection kit, Lipo8000 transfection reagent, and Radio Immuno Precipitation Assay (RIPA) analysis solution were purchased (Beyotime Company, Shanghai, China). Fetal bovine serum was purchased (PAN Company, Germany). RSL3, FER-1, and DDP were purchased (Selleck Company, USA). Mouse monoclonal antibodies against β-actin and GAPDH were purchased (Abclonal Company, Wuhan, China). Rabbit anti-GCLC was purchased (Bimake Company, USA). Rabbit secondary antibody and rat secondary antibody were purchased (Zhongshan Jinqiao Company, Beijing, China).

Cell culture

NP69 and NP69/DDP cells were placed in RPMI-1640 medium containing 10% fetal bovine serum and 1% and incubated at 37 ℃ in 5% CO_2 in a constant temperature incubator. When the cell density was 80–90%, the cells were digested and subcultured with trypsin at a concentration of 0.25%.

Western blot assay

NP69 and NP69/DDP cells at logarithmic growth stage were obtained. NP69 cells transfected with negative control plasmid and GCLC overexpressed plasmid were treated with DDP (5 μg/mL), RSL3 (2 μg/mL), or DDP+RSL3 for 48 h. Cells were then washed twice with PBS. An appropriate amount of RIPA lysate was added and placed on ice for 30 min for pyrolysis at 4 ℃ at 12,000 r/min with a centrifuge radius of 13.5 cm. After centrifugation for 15 min, the supernatant was collected and 5× protein loading buffer was added for sample preparation. The improved PVDF membrane was sealed with 5% skim milk powder at room temperature for 1h, and then the primary antibody was incubated at 4 ℃ overnight. On the second day, the PVDF membranes were washed with TBST 3 times for 10 min each time. Membranes were subsequently incubated at room temperature for 1h in the secondary antibody chamber, then washed with TBST, 3 times for 10 min each time.

Statistical analysis

Statistical data were analyzed by SPSS 23.0 software, quantitative data were represented, independent sample *t*-test for comparisons between two groups, One-way ANOVA between multiple groups, and LSD-*t*-test for pairwise comparisons between groups. Prism 7 statistical analysis was used for target genes, and one-way analysis of variance (one-way ANOVA) test was used for comparison between groups, and the test level was set at 0.05 except as otherwise indicated.

Results

Acquisition of lncRNAs associated with ferroptosis in nasopharyngeal carcinoma

Nasopharyngeal carcinoma gene expression data were obtained from TCGA database, including 535 tumor samples and 59 normal or paracancerous samples. The gene expression data of nasopharyngeal carcinoma contained 14,086 lncRNAs. Ferroptosis-related genes obtained from FerrDb (http://www.zhounan.org/ferrdb/) Co-expression analysis of nasopharyngeal carcinoma lncRNAs and nasopharyngeal carcinoma ferroptosis related-genes was performed, and 1,962 lncRNAs were obtained.

Differential lncRNAs related to the prognosis of nasopharyngeal carcinoma

In this study, the Wilcoxon test was performed on lncRNAs associated with ferroptosis in nasopharyngeal carcinoma, and 669 lncRNAs were found to be different in terms of expression between nasopharyngeal carcinoma tumor samples and normal samples. Combined with TCGA data, 14 differentially expressed lncRNAs were obtained by univariate Cox regression analysis, including 9 high-risk lncRNAs and 5 low-risk lncRNAs (*Figure 1*).

Construction and evaluation of the prognostic model

A total of 14 lncRNAs with different prognostic outcomes were included in the multivariate Cox regression analysis,

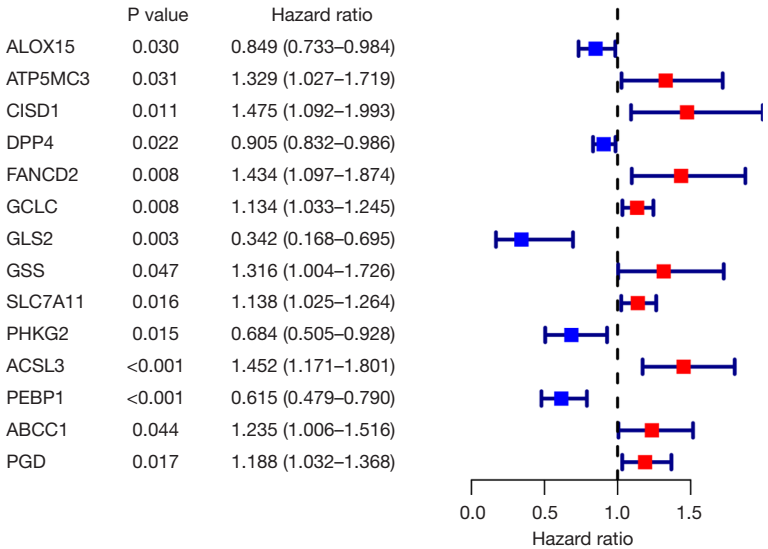

Figure 1 Differential lncRNAs in ferroptosis prognosis in nasopharyngeal carcinoma. Univariate Cox regression analysis was used to determine the prognostic differences of 14 lncRNAs and their HR (95% CI) and P values (P<0.05). Nine high-risk lncRNAs and 5 low-risk lncRNAs were included. lncRNA, long non-coding RNA.

and a multivariate prognostic risk model of the 14 lncRNAs was established, including 9 high-risk lncRNAs and 5 low-risk lncRNAs. Kaplan-Meier survival analysis of the model showed that the prognosis of the high-risk group was significantly worse than that of the low-risk group (P<0.001). Receiver operating characteristic (ROC) curve of the model was drawn, and the areas under the curve (AUCs) at 1, 2, 3, and 5 years were 0.761, 0.734, 0.738, and 0.731, respectively. Independent prognostic analysis of the model showed that P values of stage and risk score were less than 0.05 in the univariate and multivariate independent prognostic analyses (*Figure 2*). The distribution of risk scores for all patients and the relationship between risk scores and survival time suggest that patients in the high-risk group may have a shorter survival time. A heat map of lncRNA expression in the high- and low-risk groups was also generated (*Figure 3*).

Analysis of GO and KEGG enrichment

According to the risk model, the differential genes in the high-risk and low-risk groups were extracted, and GO and KEGG enrichment analyses were performed for the differential genes. GO enrichment analysis showed that the differential genes were mainly enriched in biological functions such as ciliary movement, protein processing, antibacterial body fluid reaction, cell adhesion, hormone activity, heme binding, redox enzyme activity, and iron ion binding. KEGG enrichment analysis showed that the differential genes were mainly enriched in neutrophil extracellular germicidal network, complement pathway, nitrogen metabolism, arachidonic acid metabolism, retinol metabolism, renin-angiotensin system, and fructose and mannose metabolism (*Figure 4*).

State of immune function

To explore the relationship between the prognosis and immune status of nasopharyngeal carcinoma, we used Timer, CIBERSORT, CIBERSORT-ABS, and other software to predict the differences of various immune cells in the high- and low-risk groups, and the results were as follows: immune cells such as B cells, $CD4^+$ T cells, $CD8^+$ T cells, and myeloid dendritic cells were different in the high- and low-risk groups in most of the prediction software. The single sample gene set enrichment analysis (ssGSEA) algorithm was used to quantify the infiltration scores of immune cells and disease-free related functions in the 2 groups of patients at high and low risk. Correlation analysis of immune cell subsets showed that the scores of immune cell subsets (Including dendritic cells, B cells, mast cells, neutrophils, helper T cells, and tumor-infiltrating lymphocytes) were significantly different between the high- and low risk-groups (P<0.001). In addition, there were

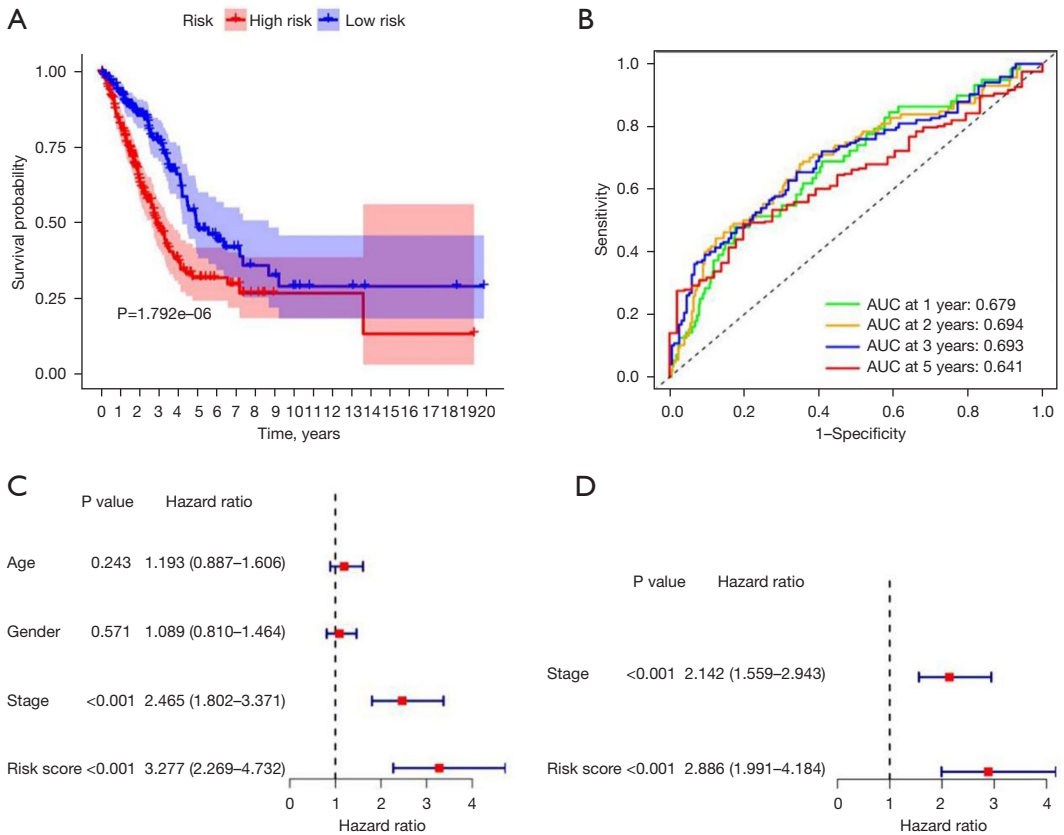

Figure 2 Evaluation of the predictive value of the prognostic model. (A) Kaplan-Meier survival analysis in the high- and low-risk group (P<0.001); (B) ROC curve of the prognostic model; (C) univariate independent prognostic analysis of the prognostic model; (D) multivariate independent prognostic analysis of the prognostic model. AUC, area under the curve; ROC, receiver operating characteristic.

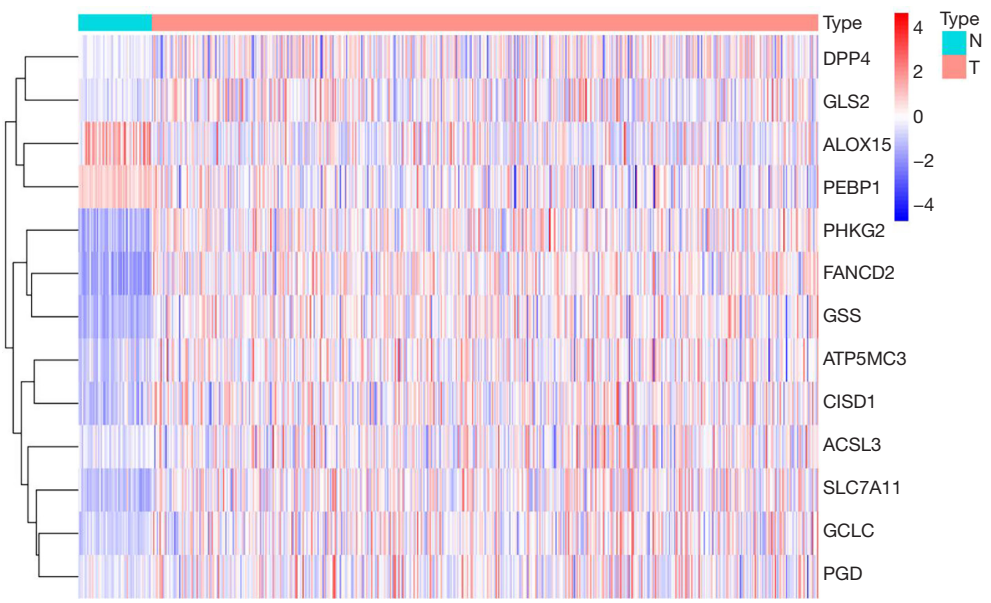

Figure 3 Heat map of 13 lncRNAs in the high- and low-risk groups. lncRNA, long non-coding RNA. N, normal; T, tumor.

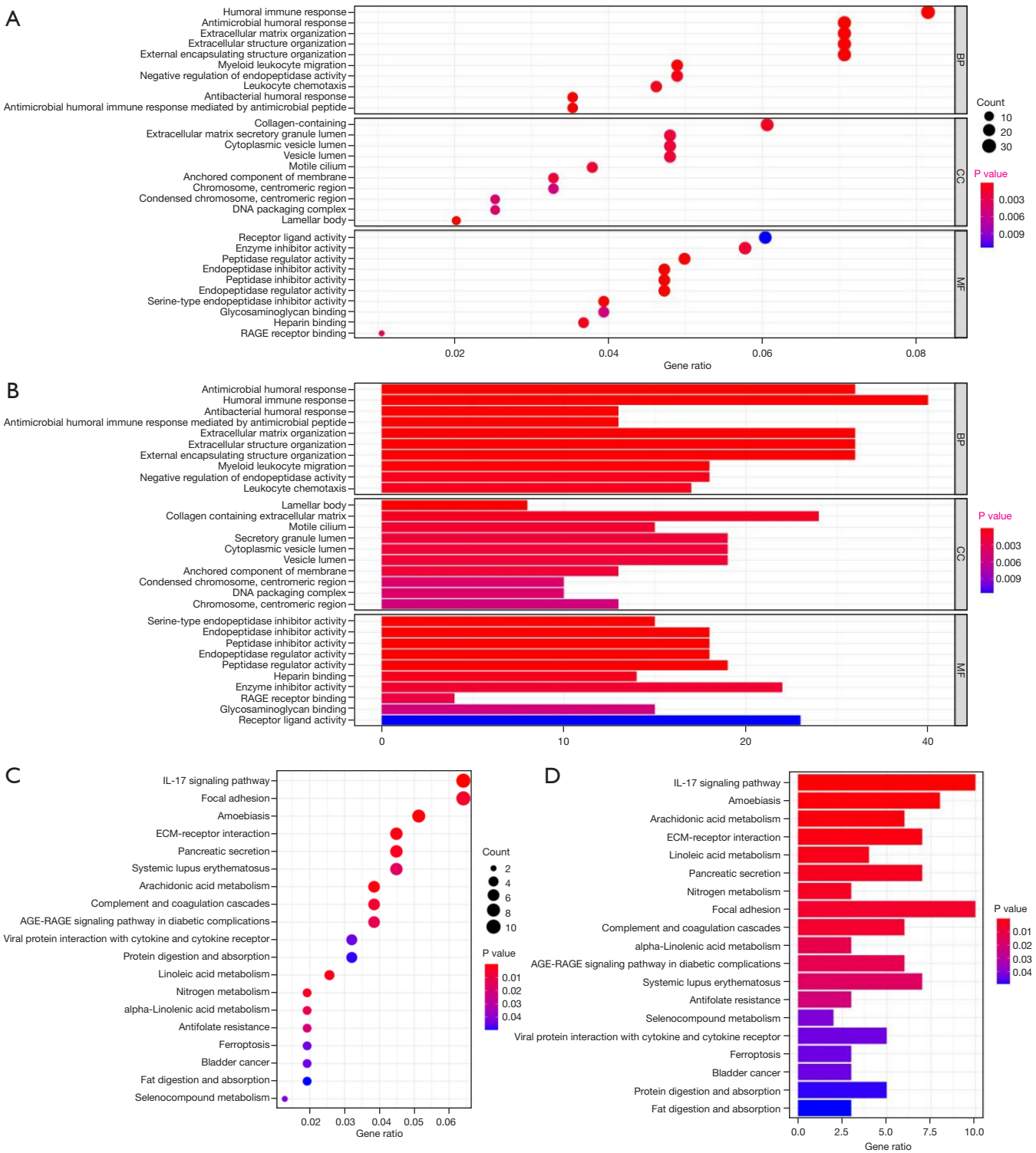

Figure 4 GO and KEGG enrichment analysis of differential genes in the high- and low-risk groups. (A) Bubble chart of GO enrichment analysis; (B) Bar graph of GO enrichment analysis; (C) Bubble chart of KEGG enrichment analysis; (D) Bar graph of KEGG enrichment analysis. BP, biological process; CC, cellular component; MF, molecular function; IL-17, interleukin 17; ECM, electro chemical machining; GO, Gene Ontology; KEGG, Kyoto Encyclopedia of Genes and Genomes.

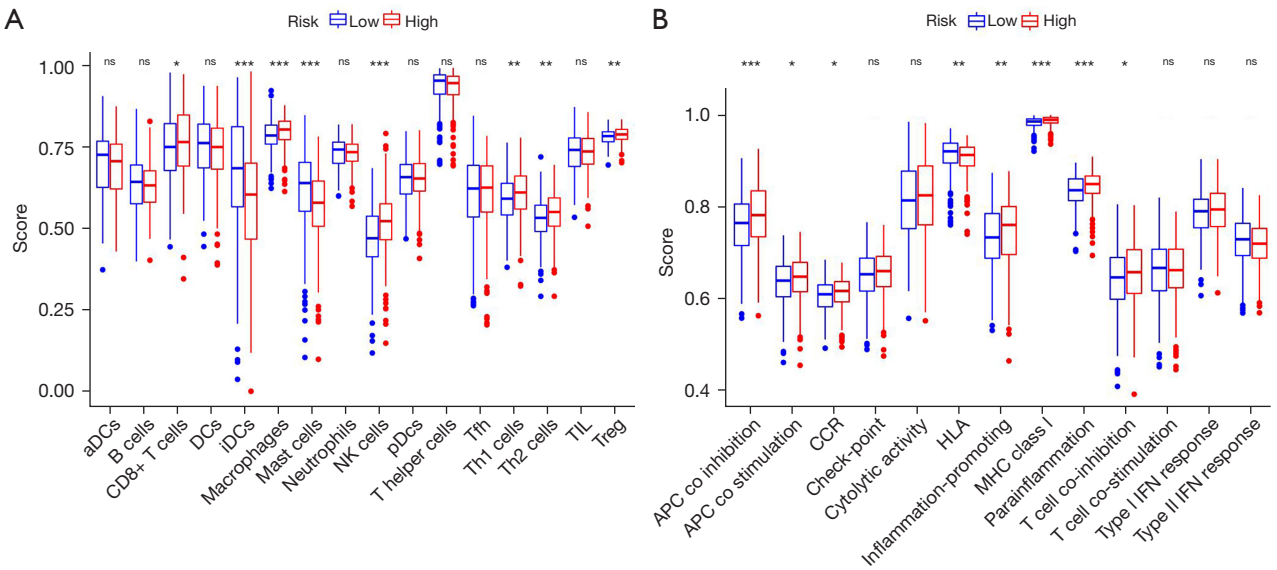

Figure 5 Immunological analysis between high- and low-risk groups. (A) Differences in immune cell subpopulation scores in the high- and low-risk groups; (B) differences in immune function scores between the high- and low-risk groups. ns, non-significance; *, P<0.05; **, P<0.01; ***, P<0.001. NK, natural killer; TIL, tumor infiltrating lymphocyte; APC, antigen presenting cell; CCR, clinical complete remission; HLA, human leukocyte antigen; MHC, major histocompatibility complex.

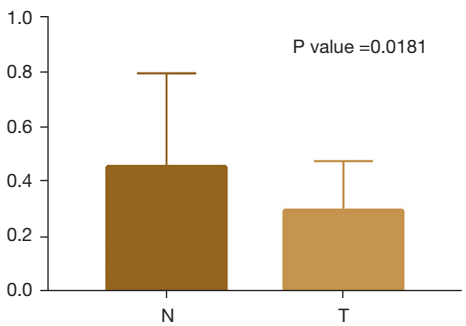

Figure 6 Comparison of *GCLC* gene expression in nasopharyngeal carcinoma tissues and normal tissues. N, normal; T, tumor; GCLC, glutamate cysteine ligase catalytic.

significant differences in immune function scores in the high- and low-risk groups, including APC co-inhibition, APC co-stimulation, chemokine receptors, immune checkpoints, human leukocyte antigen, T cell co-inhibition, T cell co-stimulation, and type II interferon response (P<0.01). In terms of the differential analysis of immune checkpoints, there were significant differences in related genes including *GCLC*, *HHLA2*, *CD276*, *BTLA*, *ICOS*, *HAVCR2*, *TNFSF15*, *LAIR1*, *TNFRSF14*, *ADORA2A*, and another 25 immune checkpoints in the high- and low-risk groups (P<0.001; *Figure 5*).

RT-PCR analysis of the GCLC gene

In this study, the expression of the *GCLC* gene in nasopharyngeal carcinoma tissues was verified by RT-PCR (polymerase chain reaction). Results of RT-PCR are generally presented in the form of mean ± standard deviation. Relative definite Halo analysis was used to analyze the results, and the 2-δ δ CT method was used to obtain the expression level of the target gene, with β-actin as the reference gene and lncRNA vim-ASL as the target gene. The measurement of the expression level of each gene was repeated twice (*Figure 6*).

Immunohistochemical analysis

The nasopharyngeal carcinoma tissue was fixed with 4% formaldehyde, embedded in paraffin, and cut into 4 μm thick sections. After melting the wax at 60 ℃, xylene dewaxing, and ethanol gradient dehydration, high pressure antigen repair was performed. The primary antibody anti-HAS-2 (1:200) was incubated on sections overnight, and the secondary antibody (horseradish peroxidase labeled) was incubated for 20 min, followed by color rendering with

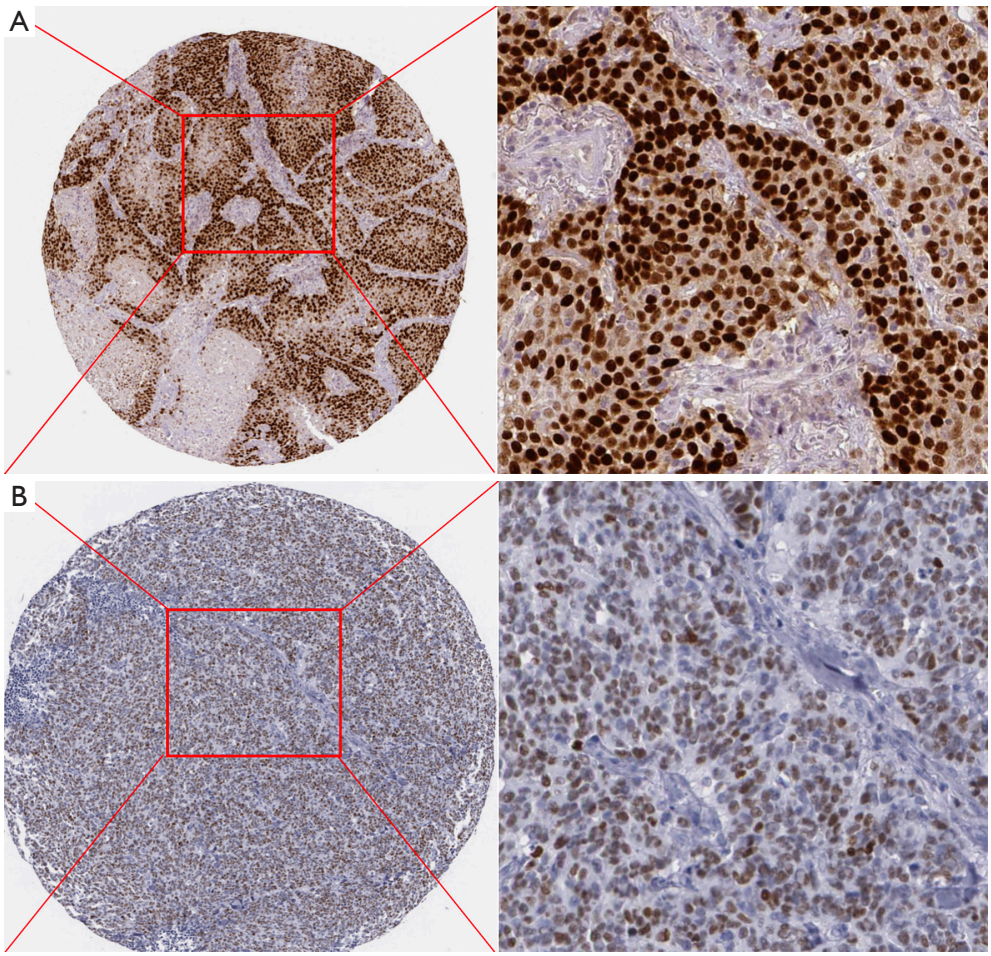

Figure 7 The relationship between GCLC expression level and clinicopathological features of nasopharyngeal carcinoma patients. (A) Frozen tumor tissue samples; (B) Fresh tumor tissue specimen. Staining method: HE; magnification (left, ×100; right, ×200). GCLC, glutamate cysteine ligase catalytic; HE, hematoxylin-eosin.

DAB solution, hematoxylin restaining, ethanol gradient dehydration, transparency, and slide sealing. Sections were examined under a microscope (×200). Positive staining was brownish yellow, 5 fields were randomly selected, and Image J software was used to analyze the area of positive staining (*Figure 7*).

Cell immunofluorescence assay

The determination of luciferase activity showed that miR-181D-5p could target GCLC because of the specific binding site R-181D-5p between GCLC 3'-UTR. We used dual luciferase gene detection and verified that GCLC is the direct target gene of miR-181D-5p. Luciferase activity of miR-181D-5p mimics ($P<0.05$) inhibited PGCLC-WT, while pGCLC-MUT did not change ($P>0.05$). In this study, RT-PCR and Western blot were also used to detect the expression of GCLC in cell lines transfected with miR-181d-5p328 inhibitor, si-GCLC, and miR-181d-5p inhibitor + si-GCLC (*Figure 8*).

Discussion

Sorafenib is a novel multi-targeted oral agent for treating tumors which selectively targets certain receptors that play a role during tumor growth (15). Sorafenib is an inducer of ferroptosis, and it was previously found that sorafenib-induced ferroptosis is unaffected by the intracellular oncogenic status, which was able to directly bind and inactivate it without affecting the level of gonad-stimulating hormone (GSH) (16). GCLC is a core target in the process of ferroptosis. Nasopharyngeal carcinoma is a highly

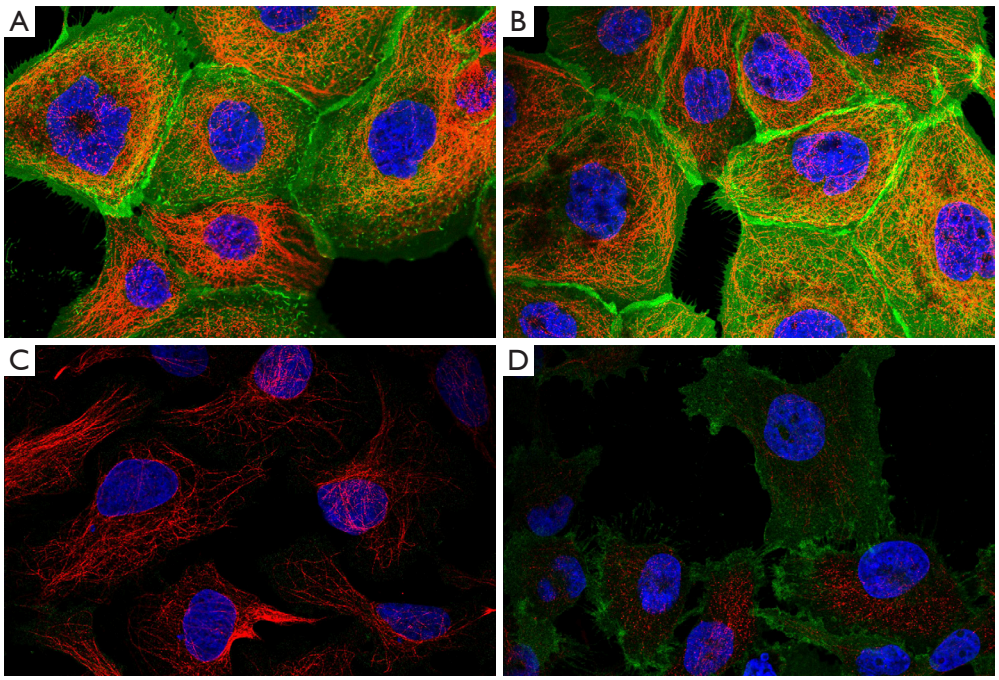

Figure 8 Cellular immunofluorescence of GCLC gene expression. Fluorescent staining of tumor tissue and cell specimens: (A) 1 h; (B) 6 h; (C) 12 h; (D) 24 h. Magnification ×400. GCLC, glutamate cysteine ligase catalytic.

malignant tumor originating from neuro-melanocytes, accounting for 1% of systemic malignancies. It is prone to lymph node metastasis or blood dissemination and has a poor prognosis, causing great harm to health (17). The low incidence of nasopharyngeal carcinoma in China may be related to the relatively low intensity of ultra violet (UV) exposure in China, and it may also be caused by data defects from the imperfect statistical reporting system. The incidence of nasopharyngeal carcinoma has increased rapidly in China and Japan, especially in men in China, with an incidence of about 20,000 new cases per year, thereby increasing the health burden (18).

Data from the WHO International Center for Cancer Research showed that men in East Asian countries (19). It has also been reported that the proportion of men and women with crude nasopharyngeal carcinoma in China is 1:0.93. In recent years, about 132,000 nasopharyngeal carcinomas cases have occurred worldwide (20). With the depletion of ozone, the atmospheric protection against ultraviolet light has become increasingly weak. It is estimated that every 10% reduction in the ozone layer will result in 4,500 patients with nasopharyngeal carcinoma (21-24). In terms of different ethnic groups, Caucasians have a much higher probability of nasopharyngeal carcinoma than other ethnic groups, 90% being primary nasopharyngeal carcinoma (25), while Asians and people of color with malignant nasopharyngeal carcinoma account for about 50–70% of primary nasopharyngeal carcinoma (26). In addition, a family history of skin cancer and long excessive exposure of skin to the sun will also increase the risk of the disease (27). Strict modeling process requires data to be divided into training sets and test sets, and test sets do not participate in the process of training model parameters (including hyperparameters). For models that do not need to select hyperparameters (such as generalized linear model or tree model when the variables have been determined), relatively reliable parameters can be obtained by training directly with training sets. However, in the case of determining hyperparameters [such as support vector machine (SVM) model, generalized linear model or tree model requiring variable screening], the training set must be further divided into a part of the validation set to determine the hyperparameters. At this point, internal verification is a very important link. In addition, when the sample size is not large enough and the test set is missing (when the sample size is small, forcibly dividing the test set may cause test deviation), the strategy of internal verification is also needed. However, due to the limitation of follow-up time,

this study cannot be verified externally.

Ferroptosis is a modified form of iron-dependent necrosis. A previous study has found that ferroptosis is associated with many human diseases, including ischemic organ injury and cancer (28). However, its role in the occurrence and development of malignant nasopharyngeal carcinoma is still unknown (29). In this study, we found that ferroptosis can affect the growth of malignant nasopharyngeal carcinoma cells, and further studied its mechanisms (30), including apoptosis, autophagy, necrosis, ROS generation, and DNA damage. The results showed that ferroptosis inhibited the growth of malignant nasopharyngeal carcinoma cells, and the mechanism was related to DNA damage. Most of the current studies regulate cell ferroptosis progression by regulating the accumulation of lipid ROS and iron metabolism (31-33). Meanwhile, stabilizing the intracellular GSH concentration also protects cells from the lipid peroxidation reaction and subsequently suppresses the ferroptosis process (34). In this study, we found that S1R is a negative regulator of ferroptosis in human nasopharyngeal carcinoma cells, which can regulate the expression of key molecules in ferroptosis, such as GSH and GCLC (35).

In this study, we demonstrate for the first time that ferroptosis process in nasopharyngeal carcinoma cells. Haloperidol regulates both GSH and GCLC expression by inhibiting S1R, thereby enhancing the anticancer effects of sorafenib.

Acknowledgments

Funding: None.

Footnote

Reporting Checklist: The authors have completed the TRIPOD reporting checklist. Available at https://tcr.amegroups.com/article/view/10.21037/tcr-22-1196/rc

Data Sharing Statement: Available at https://tcr.amegroups.com/article/view/10.21037/tcr-22-1196/dss

Conflicts of Interest: Both authors have completed the ICMJE uniform disclosure form (available at https://tcr.amegroups.com/article/view/10.21037/tcr-22-1196/coif). The authors have no conflicts of interest to declare.

Ethical Statement: The authors are accountable for all aspects of the work in ensuring that questions related to the accuracy or integrity of any part of the work are appropriately investigated and resolved. The study was conducted in accordance with the Declaration of Helsinki (as revised in 2013).

References

1. Wang W, Green M, Choi JE, et al. CD8+ T cells regulate tumour ferroptosis during cancer immunotherapy. Nature 2019;569:270-4.
2. Zhou B, Zhang JY, Liu XS, et al. Tom20 senses iron-activated ROS signaling to promote melanoma cell pyroptosis. Cell Res 2018;28:1171-85.
3. Tsoi J, Robert L, Paraiso K, et al. Multi-stage Differentiation Defines Melanoma Subtypes with Differential Vulnerability to Drug-Induced Iron-Dependent Oxidative Stress. Cancer Cell 2018;33:890-904.e5.
4. Yang Y, Luo M, Zhang K, et al. Nedd4 ubiquitylates VDAC2/3 to suppress erastin-induced ferroptosis in melanoma. Nat Commun 2020;11:433.
5. Luo M, Wu L, Zhang K, et al. miR-137 regulates ferroptosis by targeting glutamine transporter SLC1A5 in melanoma. Cell Death Differ 2018;25:1457-72.
6. Rieber M, Gomez-Sarosi LA, Rieber MS. Nitroprusside induces melanoma ferroptosis with serum supplementation and prolongs survival under serum depletion or hypoxia. Biochem Biophys Res Commun 2020;525:626-32.
7. Zhang K, Wu L, Zhang P, et al. miR-9 regulates ferroptosis by targeting glutamic-oxaloacetic transaminase GOT1 in melanoma. Mol Carcinog 2018;57:1566-76.
8. Liu L, Dong Z, Lei Q, et al. Inactivation/deficiency of DHODH induces cell cycle arrest and programed cell death in melanoma. Oncotarget 2017;8:112354-70.
9. Zhang N, Song J, Liu Y, et al. Photothermal therapy mediated by phase-transformation nanoparticles facilitates

delivery of anti-PD1 antibody and synergizes with antitumor immunotherapy for melanoma. J Control Release 2019;306:15-28.
10. Yao F, Cui X, Zhang Y, et al. Iron regulatory protein 1 promotes ferroptosis by sustaining cellular iron homeostasis in melanoma. Oncol Lett 2021;22:657.
11. Shekoohi S, Rajasekaran S, Patel D, et al. Knocking out alpha-synuclein in melanoma cells dysregulates cellular iron metabolism and suppresses tumor growth. Sci Rep 2021;11:5267.
12. Rybka JD. Radiosensitizing properties of magnetic hyperthermia mediated by superparamagnetic iron oxide nanoparticles (SPIONs) on human cutaneous melanoma cell lines. Rep Pract Oncol Radiother 2019;24:152-7.
13. Dörschmann P, Apitz S, Hellige I, et al. Evaluation of the Effects of Fucoidans from Fucus Species and Laminaria hyperborea against Oxidative Stress and Iron-Dependent Cell Death. Mar Drugs 2021;19:557.
14. Chen W, Zuo F, Zhang K, et al. Exosomal MIF Derived From Nasopharyngeal Carcinoma Promotes Metastasis by Repressing Ferroptosis of Macrophages. Front Cell Dev Biol 2021;9:791187.
15. Xie Y, Chen G. Dioscin induces ferroptosis and synergistic cytotoxicity with chemotherapeutics in melanoma cells. Biochem Biophys Res Commun 2021;557:213-20.
16. Vara-Pérez M, Rossi M, Van den Haute C, et al. BNIP3 promotes HIF-1α-driven melanoma growth by curbing intracellular iron homeostasis. EMBO J 2021;40:e106214.
17. Zhai T, Zhong W, Gao Y, et al. Tumor Microenvironment-Activated Nanoparticles Loaded with an Iron-Carbonyl Complex for Chemodynamic Immunotherapy of Lung Metastasis of Melanoma In Vivo. ACS Appl Mater Interfaces 2021;13:39100-11.
18. Liao Y, Jia X, Ren Y, et al. Suppressive role of microRNA-130b-3p in ferroptosis in melanoma cells correlates with DKK1 inhibition and Nrf2-HO-1 pathway activation. Hum Cell 2021;34:1532-44.
19. Filipczak N, Jaromin A, Piwoni A, et al. A Triple Co-Delivery Liposomal Carrier That Enhances Apoptosis via an Intrinsic Pathway in Melanoma Cells. Cancers (Basel) 2019;11:1982.
20. Wang S, Yi X, Wu Z, et al. CAMKK2 Defines Ferroptosis Sensitivity of Melanoma Cells by Regulating AMPK–NRF2 Pathway. J Invest Dermatol 2022;142:189-200.e8.
21. Capitao M, Perrin J, Simon S, et al. Anti-Tumor Efficacy of PD-L1 Targeted Alpha-Particle Therapy in a Human Melanoma Xenograft Model. Cancers (Basel) 2021;13:1256.
22. Knackstedt RW, Knackstedt T, Gastman B. Gene expression profiling in melanoma: past results and future potential. Future Oncol 2019;15:791-800.
23. Ahmed B, Qadir MI, Ghafoor S. Malignant Melanoma: Skin Cancer-Diagnosis, Prevention, and Treatment. Crit Rev Eukaryot Gene Expr 2020;30:291-7.
24. Marchetti MA, Coit DG, Dusza SW, et al. Performance of Gene Expression Profile Tests for Prognosis in Patients With Localized Cutaneous Melanoma: A Systematic Review and Meta-analysis. JAMA Dermatol 2020;156:953-62.
25. Arozarena I, Wellbrock C. Phenotype plasticity as enabler of melanoma progression and therapy resistance. Nat Rev Cancer 2019;19:377-91.
26. Tian M, Yang J, Han J, et al. A novel immune checkpoint-related seven-gene signature for predicting prognosis and immunotherapy response in melanoma. Int Immunopharmacol 2020;87:106821.
27. Gao Y, Li Y, Niu X, et al. Identification and Validation of Prognostically Relevant Gene Signature in Melanoma. Biomed Res Int 2020;2020:5323614.
28. Wan Q, Tang J, Han Y, et al. Co-expression modules construction by WGCNA and identify potential prognostic markers of uveal melanoma. Exp Eye Res 2018;166:13-20.
29. Huang R, Mao M, Lu Y, et al. A novel immune-related genes prognosis biomarker for melanoma: associated with tumor microenvironment. Aging (Albany NY) 2020;12:6966-80.
30. Fröhlich A, Sirokay J, Fietz S, et al. Molecular, clinicopathological, and immune correlates of LAG3 promoter DNA methylation in melanoma. EBioMedicine 2020;59:102962.
31. Azevedo H, Pessoa GC, de Luna Vitorino FN, et al. Gene co-expression and histone modification signatures are associated with melanoma progression, epithelial-to-mesenchymal transition, and metastasis. Clin Epigenetics 2020;12:127.
32. Wan Q, Jin L, Su Y, et al. Development and validation of autophagy-related-gene biomarker and nomogram for predicting the survival of cutaneous melanoma. IUBMB Life 2020;72:1364-78.
33. Monteiro AC, Muenzner JK, Andrade F, et al. Gene expression and promoter methylation of angiogenic and lymphangiogenic factors as prognostic markers in melanoma. Mol Oncol 2019;13:1433-49.
34. Ercin ME, Bozdoğan Ö, Çavuşoğlu T, et al. Hypoxic

Gene Signature of Primary and Metastatic Melanoma Cell Lines: Focusing on HIF-1β and NDRG-1 Balkan Med J 2019;37:15-23.
35. Christensen JN, Schmidt H, Steiniche T, et al. Identification of robust reference genes for studies of gene expression in FFPE melanoma samples and melanoma cell lines. Melanoma Res 2020;30:26-38.

(English Language Editor: C. Betlazar-Maseh)

Cite this article as: Dai Z, Zhong Y. Bioinformatics analysis based on ferroptosis-related lncRNAs: construction of a clinical prognostic model for nasopharyngeal carcinoma and correlation analysis. Transl Cancer Res 2022;11(6):1665-1677. doi: 10.21037/tcr-22-1196

